# Ultrafast dynamics of electrons excited by femtosecond laser pulses: Spin polarization and spin-polarized currents

Oliver Busch,* Franziska Ziolkowski, Ingrid Mertig, and Jürgen Henk
*Institut für Physik, Martin Luther University Halle-Wittenberg, 06099 Halle, Germany*

(Received 26 April 2023; accepted 16 October 2023; published 2 November 2023)

Laser radiation incident on a ferromagnetic sample produces excited electrons and currents whose spin polarization must not be aligned with the magnetization—an effect due to spin-orbit coupling that is ubiquitous in spin- and angle-resolved photoemission. In this paper, we report on a systematic investigation of the dynamics of spin polarization and spin-polarized currents produced by femtosecond laser pulses, modeled within our theoretical framework EVOLVE. The spin polarization depends strongly on the properties of the laser pulse and on the sample composition, as shown by comparing results for Cu(100), Co(100), and a Co/Cu heterostructure. We find a transition from coherence before the laser pulse's maximum to incoherence thereafter. Moreover, the time dependence of the spin-polarization components induced by spin-orbit coupling differ significantly in Cu and Co: in Cu, we find long-period oscillations with tiny rapid modulations, whereas in Co prominent rapid oscillations with long-period ones are superimposed. The pronounced spatial dependences of the signals underline the importance of inhomogeneities; in particular, magnetic/nonmagnetic interfaces act as a source for ultrafast spin-polarization effects. Our investigation provides detailed insight into electron dynamics during and shortly after a femtosecond laser excitation.

DOI: 10.1103/PhysRevB.108.184401

## I. INTRODUCTION

Spin-polarized photocurrents are ubiquitous in spin- and angle-resolved photoelectron spectroscopy (SARPES) [1,2]. In nonmagnetic samples, the spin polarization of the detected photocurrents—brought about by spin-orbit coupling—depends on details of the setup, in particular on those of the incident electromagnetic radiation (e.g., on photon energy, polarization, and incidence direction; see, for example, Ref. [3]) and on the symmetry of the surface [4–7]. In magnetic samples, the same effect results in magnetic dichroism [8,9], and as theoretical and experimental studies have shown, the spin-orbit-induced spin polarization *of photoelectrons* must not be aligned with the magnetization direction (see, for example, Ref. [8] and references therein).

In ultrafast spin dynamics, electrons are excited by electromagnetic radiation as well, for example, by a femtosecond laser pulse. Focusing on the demagnetization of a magnetic sample [10–12], one investigates mainly the reduction in the magnetization and disregards its change in direction. The latter could be brought about by photoinduced spin-polarization components that are not aligned with the ground state's magnetization. In SARPES these "oblique" components are those of electrons measured *at a detector*, whereas in ultrafast spin dynamics they are those of electrons *within a sample*; thus, one is concerned with different boundary conditions [13]. This idea immediately calls for a systematic investigation of photoinduced spin polarization and spin-polarized currents caused by femtosecond laser pulses.

Ultrafast spin currents have been studied for more than a decade, for example, in terms of superdiffusive spin currents. Battiato and coworkers focused on the density of hot majority carriers [14–16]. The dynamics of the spin currents is calculated using spin-dependent scattering rates and spin-dependent transmission of the interface, while the excitation is treated as a source term. Other semiclassical approaches are based on the Boltzmann transport equation, as in the work by Nenno *et al.* [17], or on a wave-diffusion equation, as in the work by Kaltenborn *et al.* [18].

In the theoretical study reported in this paper, we concentrate on the spin-orbit-induced spin-polarization effects during and shortly after a laser excitation. In order to determine the main features we begin with a nonmagnetic sample, Cu(100), and then turn to a magnetic sample, fcc Co(100). Since real samples often contain interfaces, we investigate the role of the latter by means of a Co/Cu(100) heterostructure.

Questions worth considering are, among others, which components of the spin polarization are forbidden by symmetry? How large are the allowed components, and are their magnitudes comparable to those observed in SARPES? What are their temporal and spatial distributions? Does magnetism reduce the oblique spin-orbit-induced components (here in samples containing Co)? What are the detailed properties of the photoinduced currents? We respond to these questions in this work.

The simulations were performed using our computational framework EVOLVE [19,20]. In contrast to the established approaches mentioned above, EVOLVE goes beyond the two-current model. Moreover, details of the laser radiation are taken into account, with excitations included in the electric dipole approximation. On the other hand, scattering processes

*Corresponding author: oliver.busch@physik.uni-halle.de

 

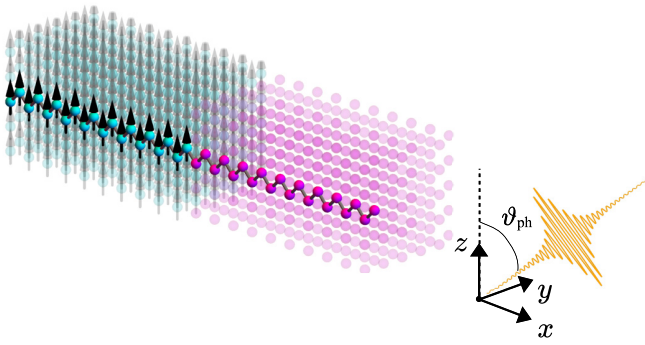


FIG. 1. Geometry of a Co/Cu heterostructure. The fcc film consists of 40 layers stacked in the $x$ direction, with 20 layers of Co atoms (cyan spheres) and 20 layers of Cu atoms (magenta spheres). The Co magnetic moments point along the $z$ direction (black arrows). The film is infinite in the $y$ and $z$ directions but finite in the $x$ direction. Sites with intense color forming a zigzag chain belong to one unit cell of the slab. A laser pulse impinges with a polar angle $\vartheta_{\rm ph}$ of 45 ° within the $xz$ plane onto the sample.

are not considered on the microscopic level, but coupling to a bosonic heat bath allows for relaxation of the excited state toward the thermal ground state.

This paper is organized as follows. In Sec. II we sketch our approach to ultrafast electron dynamics (Sec. II A), discuss spin polarization as well as currents (Sec. II B), and perform a symmetry analysis (Sec. II C). Results are discussed in Sec. III: beginning with Cu(100) (Sec. III A), we turn then to magnetic systems, namely, fcc Co(100) (Sec. III B) and a Co/Cu(100) heterostructure (Sec. III C). We conclude in Sec. IV.

## II. THEORETICAL ASPECTS

### A. Ultrafast electron dynamics

The samples are freestanding fcc(100) films 40 layers thick. We consider Cu(100), Co(100), and Co/Cu(100) (with 20 layers each) films. The Cartesian $x$ axis is perpendicular to the film, and we apply periodic boundary conditions within the film, i.e., in the $y$ and $z$ directions. In the case of Co(100) and Co/Cu(100), the magnetic moments are collinear and point along the $z$ direction (Fig. 1) [21].

Co grows epitaxially on Cu(100), so that Co films adopt the in-plane lattice of Cu(100) but are tetragonally distorted (face-centered tetragonal lattice). However, the EVOLVE computer code requires a single lattice constant, so Co regions are taken as fcc with the lattice constant of Cu (0.36 nm [22] instead of 0.34 nm found for fcc Co [23]).

The electronic structure of the samples is described by a tight-binding Hamiltonian $\hat{H}_0$ of Slater-Koster type [24], with parameters for the $s$, $p$, and $d$ orbitals taken from Ref. [25]. Collinear magnetism and spin-orbit coupling are taken into account as described in Ref. [26].

The electron system is excited by a femtosecond laser pulse with photon energy $E_{\rm ph} = \omega$ (in atomic units, $\hbar = 1$). The laser's electric field

$$\boldsymbol{E}(t) = l(t) \sum_{l={\rm s,p}} \boldsymbol{E}_l \cos(\omega t + \varphi_l) \tag{1}$$

is a coherent superposition of $s$- and $p$-polarized partial waves modulated with a Lorentzian envelope $l(t)$. $\boldsymbol{E}_l$ and $\varphi_l$ are the amplitudes and the phase shifts of the partial waves, respectively.

The electromagnetic radiation impinges within the $xz$ plane onto the films, with a polar angle $\vartheta_{\rm ph} = 45^\circ$ of incidence. For $s$-polarized light ($\boldsymbol{E}_{\rm p} = 0$), $\boldsymbol{E}(t)$ points along the $y$ axis, which is perpendicular to the plane of incidence, the latter spanned by the incidence direction of the light and the surface normal. For $p$-polarized light ($\boldsymbol{E}_{\rm s} = 0$), $\boldsymbol{E}(t)$ lies within the $xz$ incidence plane. Circularly polarized radiation with helicity $\sigma^{\pm}$ is obtained with $\varphi_{\rm s} - \varphi_{\rm p} = \pm 90^\circ$ and equal amplitudes ($E_{\rm s} = E_{\rm p}$).

Excitation with a circularly polarized laser pulse may induce a spin polarization [8], which is discussed in this work, or a magnetization, i.e., the inverse Faraday effect [27–29]. An induced magnetization creates a magnetic field that could dynamically affect the electrons and the magnetic texture of magnetic samples, thereby coupling the electron dynamics with magnetization dynamics. In the present stage of the EVOLVE framework, this feature is not incorporated.

The electron dynamics is described by the von Neumann equation

$$-i\frac{d\hat{\rho}(t)}{dt} = [\hat{\rho}(t), \hat{H}(t)] \tag{2}$$

for the one-particle density matrix

$$\hat{\rho}(t) = \sum_{n,m} |n\rangle\, p_{nm}(t)\, \langle m|. \tag{3}$$

$\{|n\rangle\}$ is the set of eigenstates of $\hat{H}_0$, with $\hat{H}_0|n\rangle = \epsilon_n|n\rangle$. The time-dependent Hamiltonian $\hat{H}(t)$ comprises the electric field of the laser via minimal coupling [30]. The equation of motion (2) for $\hat{\rho}(t)$ is solved within our theoretical framework EVOLVE; for details see Refs. [19,20].

### B. Spin polarization and spin-polarized currents

Site-, orbital-, and spin-resolved properties of an observable $O$ are obtained by taking partial traces in the expectation values $\langle O\rangle(t) = {\rm Tr}[\hat{\rho}(t)\,\hat{O}]$, with the density matrix in an appropriate basis.

In matrix form an expectation value reads $\langle O\rangle(t) = {\rm tr}[\mathsf{P}(t)\,\mathsf{O}]$. We define matrices $\mathsf{p}_{kl}^{\sigma\sigma'}$ and $\mathsf{h}_{kl}^{\sigma\sigma'}$ for the density matrix and the Hamiltonian, respectively, with elements

$$\left(\mathsf{p}_{kl}^{\sigma\sigma'}\right)_{\alpha\beta} = p_{k\alpha\sigma,l\beta\sigma'}, \tag{4a}$$

$$\left(\mathsf{h}_{kl}^{\sigma\sigma'}\right)_{\alpha\beta} = h_{k\alpha\sigma,l\beta\sigma'}. \tag{4b}$$

$k$ and $l$ are site indices, $\sigma$ and $\sigma'$ specify the spin orientation ($\uparrow$ and $\downarrow$ with respect to the $z$ direction), and $\alpha$ and $\beta$ are orbital indices. These matrices are combined into site-resolved block matrices

$$\mathsf{P}_{kl} = \begin{pmatrix} \mathsf{p}_{kl}^{\uparrow\uparrow} & \mathsf{p}_{kl}^{\uparrow\downarrow} \\ \mathsf{p}_{kl}^{\downarrow\uparrow} & \mathsf{p}_{kl}^{\downarrow\downarrow} \end{pmatrix}, \tag{5a}$$

$$\mathsf{H}_{kl} = \begin{pmatrix} \mathsf{h}_{kl}^{\uparrow\uparrow} & \mathsf{h}_{kl}^{\uparrow\downarrow} \\ \mathsf{h}_{kl}^{\downarrow\uparrow} & \mathsf{h}_{kl}^{\downarrow\downarrow} \end{pmatrix}. \tag{5b}$$

The spin polarization at site $l$ is given by

$$s_l^\mu = \mathrm{tr}\,(\mathsf{P}_{ll}\Sigma^\mu), \quad \mu = x, y, z,$$

in which $\Sigma^\mu$ is a block Pauli matrix. Explicitly,

$$s_l^x = 2\,\mathrm{Re}\,\mathrm{tr}\,\left(\mathsf{p}_{ll}^{\uparrow\downarrow}\right), \tag{6a}$$

$$s_l^y = -2\,\mathrm{Im}\,\mathrm{tr}\,\left(\mathsf{p}_{ll}^{\uparrow\downarrow}\right), \tag{6b}$$

$$s_l^z = \mathrm{tr}\,\left(\mathsf{p}_{ll}^{\uparrow\uparrow} - \mathsf{p}_{ll}^{\downarrow\downarrow}\right), \tag{6c}$$

with normalization $\mathrm{tr}(\mathsf{P}_{ll}) = 1$. The site-averaged spin polarization

$$S^\mu = \frac{1}{N_\mathrm{site}} \sum_l s_l^\mu, \quad \mu = x, y, z, \tag{7}$$

is obtained by summation over all $N_\mathrm{site}$ sites in a film's unit cell. Assuming a slab geometry, a unit cell consists of $N_\mathrm{site} = 40$ sites forming a zigzag chain in the $x$ direction (see the color-saturated sites belonging to one unit cell in Fig. 1).

The current

$$j_{kl} = -\frac{i}{2}\,\mathrm{tr}\,(\mathsf{P}_{lk}\mathsf{H}_{kl}) - \langle l \leftrightarrow k\rangle \tag{8}$$

from site $l$ to site $k$ and the respective spin-polarized currents

$$j_{kl}^\mu = -\frac{i}{4}\,\mathrm{tr}\,(\mathsf{P}_{lk}[\Sigma^\mu, \mathsf{H}_{kl}]_+) - \langle l \leftrightarrow k\rangle, \quad \mu = x, y, z, \tag{9}$$

are derived from Mahan's equation for the current operator in spin-symmetrized form [31] (see also Refs. [32,33]; $[\cdot,\cdot]_+$ is the anticommutator). For collinear magnetic textures, as discussed in this paper, intersite hopping with spin flip does not occur in $\hat{H}_0$, i.e., $\mathsf{h}_{kl}^{\uparrow\downarrow} = 0$ and $\mathsf{h}_{kl}^{\downarrow\uparrow} = 0$. With this information, the above equations become

$$j_{kl} = -\frac{i}{2}\,\mathrm{tr}\,\left(\mathsf{p}_{lk}^{\uparrow\uparrow}\mathsf{h}_{kl}^{\uparrow\uparrow} + \mathsf{p}_{lk}^{\downarrow\downarrow}\mathsf{h}_{kl}^{\downarrow\downarrow}\right) - \langle l \leftrightarrow k\rangle, \tag{10a}$$

$$j_{kl}^x = -\frac{i}{4}\,\mathrm{tr}\,\left(\mathsf{p}_{lk}^{\uparrow\downarrow} + \mathsf{p}_{lk}^{\downarrow\uparrow}\right)\left(\mathsf{h}_{kl}^{\uparrow\uparrow} + \mathsf{h}_{kl}^{\downarrow\downarrow}\right) - \langle l \leftrightarrow k\rangle, \tag{10b}$$

$$j_{kl}^y = \frac{1}{4}\,\mathrm{tr}\,\left(\mathsf{p}_{lk}^{\uparrow\downarrow} - \mathsf{p}_{lk}^{\downarrow\uparrow}\right)\left(\mathsf{h}_{kl}^{\uparrow\uparrow} + \mathsf{h}_{kl}^{\downarrow\downarrow}\right) - \langle l \leftrightarrow k\rangle, \tag{10c}$$

$$j_{kl}^z = -\frac{i}{2}\,\mathrm{tr}\,\left(\mathsf{p}_{lk}^{\uparrow\uparrow}\mathsf{h}_{kl}^{\uparrow\uparrow} - \mathsf{p}_{lk}^{\downarrow\downarrow}\mathsf{h}_{kl}^{\downarrow\downarrow}\right) - \langle l \leftrightarrow k\rangle. \tag{10d}$$

Interchanging the site and the spin indices yields $j_{kl} = -j_{lk}$ and $j_{kl}^\mu = -j_{lk}^\mu = j_{lk}^{-\mu}$.

### C. Symmetry analysis

Instead of a full group-theoretical analysis [8], we perform a symmetry analysis which reveals which components of the spin polarization are forbidden for a given setup. The important symmetry is the reflection $\hat{m}_y$ at the $xz$ plane: $(x, y, z) \to (x, -y, z)$ since the $xz$ plane is a symmetry plane of the lattice and is also the laser's plane of incidence (spanned by the light incidence direction and the surface normal).

For $p$-polarized light, $\hat{m}_y$ is a symmetry operation for a nonmagnetic sample ($\boldsymbol{M} = 0$; here Cu) which indicates that only $S^y$ is allowed to be nonzero (Table I). A $z$ magnetization breaks this symmetry [$\boldsymbol{M} \neq 0$; here Co(100) and Co/Cu(100)], and all three components of $\boldsymbol{S}$ are allowed to be nonzero.

TABLE I. Effect of symmetry operations on the laser's electric field $\boldsymbol{E}$ decomposed into its $s$- and $p$-polarization components $\boldsymbol{E}_\mathrm{s}$ and $\boldsymbol{E}_\mathrm{p}$, the magnetization $\boldsymbol{M}$ in the $z$ direction, and the electron spin polarization $\boldsymbol{S} = (S^x, S^y, S^z)$. $\hat{1}$ is the identity operation, and $\hat{m}_y$ is the reflection at the $xz$ plane.

| Operation | Electric field | | Magnetization | Spin polarization | | |
|---|---|---|---|---|---|---|
| $\hat{1}$ | $\boldsymbol{E}_\mathrm{s}$ | $\boldsymbol{E}_\mathrm{p}$ | $\boldsymbol{M}$ | $S^x$ | $S^y$ | $S^z$ |
| $\hat{m}_y$ | $-\boldsymbol{E}_\mathrm{s}$ | $\boldsymbol{E}_\mathrm{p}$ | $-\boldsymbol{M}$ | $-S^x$ | $S^y$ | $-S^z$ |

For $s$-polarized light, the electric field of the laser is along the $y$ direction. Since for homogeneous nonmagnetic samples (Cu) the $z$ rotation by 180° leaves the setup invariant, $S^y = 0$ and $S^z = 0$. For $S^y$ this symmetry holds for the spin polarization at each site ($s_l^y = 0$). For $S^z$, however, it holds only for the site-averaged spin polarization, that is, $s_l^z$ at equivalent sites $l$ may be nonzero but compensate each other (equivalent sites have the same distance from the two surfaces of a film).

Considering circularly polarized light, $\hat{m}_y$ reverses the helicity $\sigma^\pm \to \sigma^\mp$ [$(\boldsymbol{E}_\mathrm{s}, \boldsymbol{E}_\mathrm{p}) \to (-\boldsymbol{E}_\mathrm{s}, \boldsymbol{E}_\mathrm{p})$], which indicates that $S^x$ and $S^z$ change sign under helicity reversal for a nonmagnetic sample but $S^y$ does not. For magnetic samples this strict relation is broken, which may be regarded as a magnetic spin dichroism (magnetic dichroism is an intensity change upon magnetization reversal [34]; here we are concerned with a change in the spin polarization). The symmetry-allowed and -forbidden spin-polarization components are summarized in Table II.

## III. RESULTS AND DISCUSSION

To discuss our results, we increase the order of complexity step by step. We begin with a nonmagnetic Cu(100) film since it exhibits the phenomena most clearly. The effect of magnetism is addressed by fcc Co(100), and eventually, the combination of both systems into a Co/Cu(100) heterostructure allows an examination of the effect of a magnetic/nonmagnetic interface. For selected cases, animations of the spin dynamics are provided in the Supplemental Material [35].

In all simulations discussed below, the laser has a photon energy of 1.55 eV and a fluence of about 3.3 mJ cm$^{-2}$ and is modulated with a Lorentzian $l(t)$ 10 fs wide. All samples comprise 40 layers, with sites 0 and 39 defining the bottom

TABLE II. Components of the site-averaged electron spin polarization $\boldsymbol{S} = (S^x, S^y, S^z)$ allowed (+) or forbidden (−) by symmetry, with the magnetic case given in rectangular brackets. For details see the text.

| Polarization | $S^x$ | $S^y$ | $S^z$ |
|---|---|---|---|
| $p$ | − [+] | + [+] | − [+] |
| $s$ | − [−] | − [+] | − [+] |
| Circular | + [+] | + [+] | + [+] |

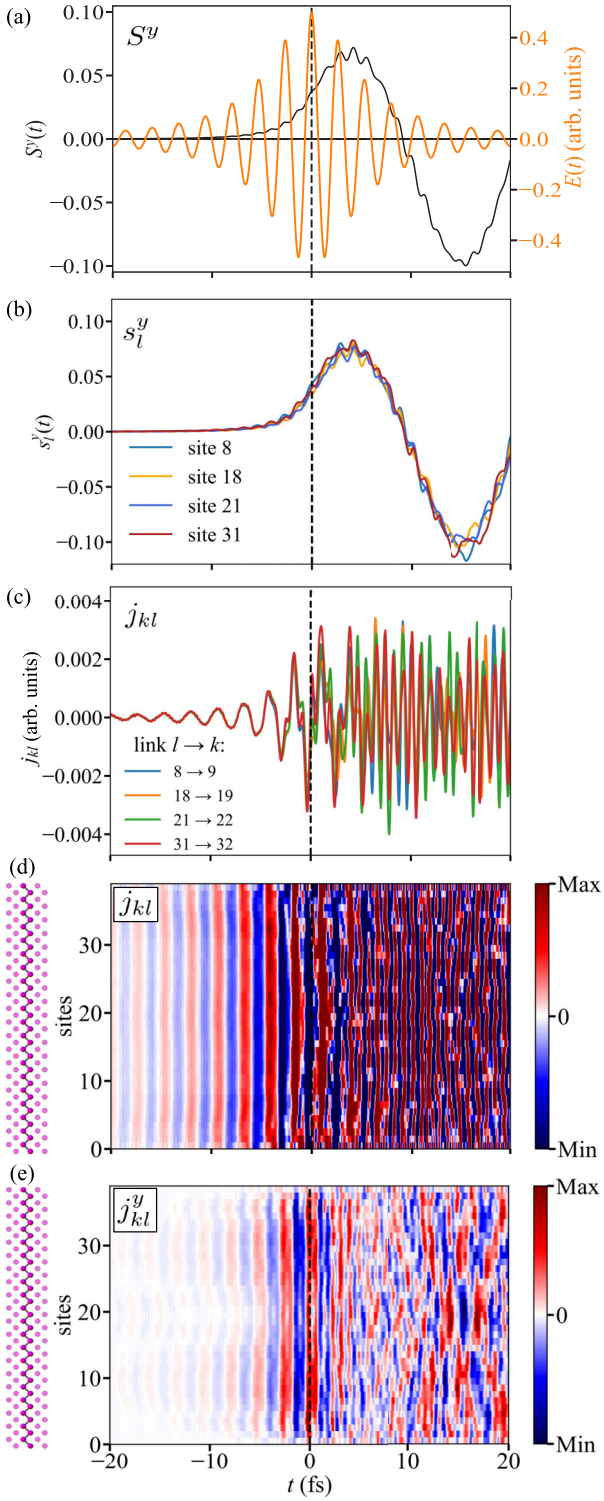


FIG. 2. Photoinduced spin polarization and currents for a Cu(100) sample excited by $p$-polarized light. (a) Site-averaged spin polarization $S^y(t)$ (black) and electric field of the laser pulse (orange; schematic). (b) Local spin polarization $s_l^y(t)$ for selected sites, as indicated. (c) Currents $j_{kl}(t)$ between neighboring sites $l \to k = l + 1$ for selected site pairs as indicated. (d) Currents $j_{kl}(t)$ and (e) spin-resolved currents $j_{kl}^y(t)$; their magnitude is indicated by color bars with the same range (red is positive; blue is negative). Data in [(c)–(e)] are in arbitrary units. Vertical dashed lines at $t = 0$ fs mark the maximum of the laser pulse.

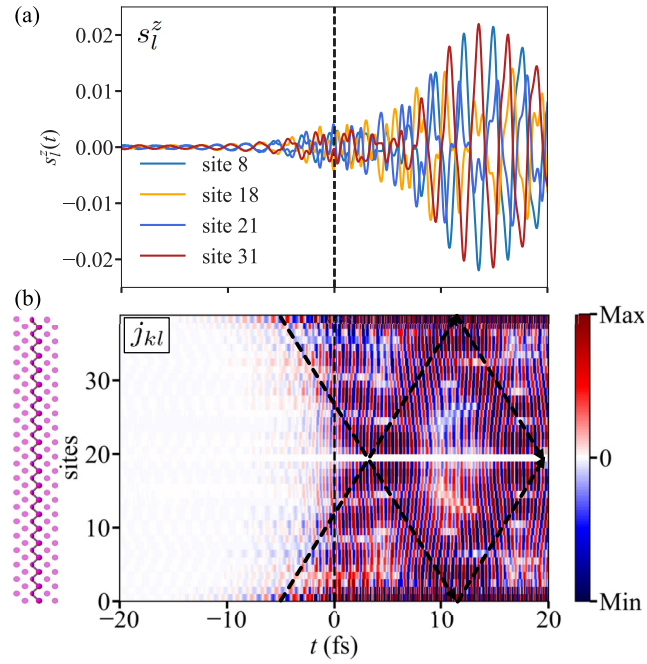


FIG. 3. Photoinduced spin polarization and current of a Cu(100) film excited by $s$-polarized light. (a) $s_l^z(t)$ for selected sites as indicated. Sites 8 (18) and 31 (21) are equivalent. (b) Currents $j_{kl}(t)$ displayed as a color scale (red is positive, and blue is negative; in arbitrary units). Dashed arrows serve as guides to the eye. Vertical dashed lines at $t = 0$ fs indicate the maximum of the laser pulse.

and top surfaces, respectively. We focus on currents across the samples, that is, along the zigzag path displayed in Fig. 1.

### A. Cu(100)

In accordance with the symmetry analysis (Table II), the calculations for $p$-polarized light yield only a nonzero $S^y$ that is slightly modulated with the doubled laser frequency [Fig. 2(a)]. The sizable magnitude is explained by the local contributions $s_l^y(t)$, which oscillate in phase with almost identical amplitudes [constructive interference; Fig. 2(b)]. After the laser pulse, deviations among the site-resolved spectra increase marginally (see $t > 12$ fs).

The above "unison" oscillations found for $s_l^y(t)$ show up as well in the currents $j_{kl}(t)$ before the laser pulse's maximum [Figs. 2(c) and 2(d)], but with a much smaller period. The laser's photon energy of 1.55 eV corresponds to a period of 2.7 fs, or about 3.7 oscillations within 10 fs, which is also seen in Figs. 2(c) and 2(d). This suggests that the electron system follows the electric field of the laser, which is a collective motion across the film (in the $x$ direction). At about $t = -3$ fs, increasing interference, starting at the surfaces, reduces the coherence in the oscillations, thereby obliterating the pattern at later times.

The oscillations of the currents are accompanied by those of the spin-resolved currents $j_{kl}^y(t)$ in opposite directions [Fig. 2(e); the $x$ and $z$ components are zero]. A current in the positive $x$ direction [red in Fig. 2(d)] appears simultaneously with a spin-polarized current in the opposite direction [blue in Fig. 2(e)], which implies a flow of $-y$-polarized electrons in

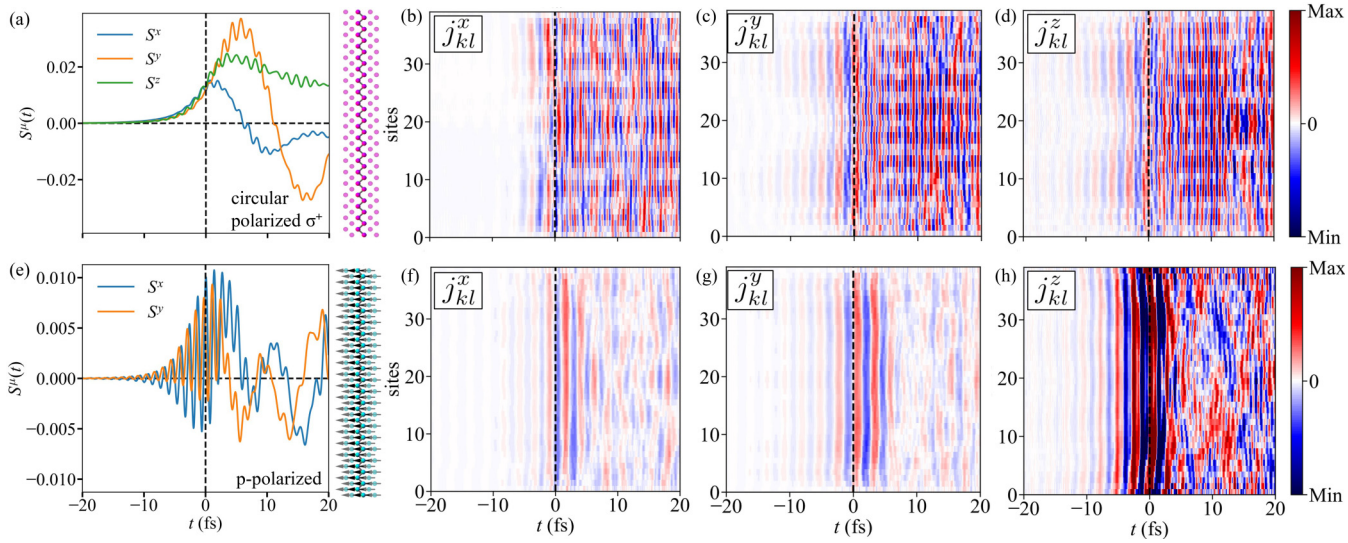


FIG. 4. Photoinduced spin polarization $S^{\mu}(t)$ and spin-resolved currents $j^{\mu}_{kl}(t)$ for a Cu(100) film excited by circularly polarized light with helicity $\sigma^+$ (top row) and for fcc Co(100) excited by $p$-polarized light (bottom row). (a) Site-averaged spin polarization $S^{\mu}(t)$ for Cu(100) ($\mu = x, y, z$). [(b)–(d)] Spin-resolved currents $j^{\mu}_{kl}(t)$ displayed as a color scale, as in Fig. 2. (e) $S^x(t)$ and $S^y(t)$ for Co(100). [(f)–(h)] The same as [(b)–(d)] using the same color scale. Dashed vertical lines indicate the maximum of the laser pulse at $t = 0$ fs.

the $x$ direction [36]. Again, the current pattern becomes complicated after the laser pulse due to the interference mentioned before.

For $s$-polarized light, the symmetry analysis yields $\boldsymbol{S} = 0$ but allows for $s^z_l \neq 0$. The photoinduced local spin polarizations at equivalent sites thus have to compensate each other. This is fully confirmed by the simulations: the spin polarization is spatially antisymmetric within the Cu film [Fig. 3(a)].

The antisymmetry of the spin polarization may be attributed to the surface normals of the freestanding Cu film being opposite to each other. This reasoning complies with spin polarization effects in spin- and angle-resolved photoemission [4–8] since they rely on the presence of a surface (they do not occur in bulk samples). Hence, one may regard the present result as an indication of the importance of surfaces and interfaces for ultrafast spin dynamics; see, for example, Ref. [19] (for reviews on polarized electrons at surfaces we refer to Refs. [37,38]).

The above argument is supported by the currents $j_{kl}(t)$ [Fig. 3(b)] which are initiated at the surfaces: compare, for example, the darker color scale at surface sites 0 and 39 in Fig. 3(b) with the lighter colors in the interior of the film at $t = -5$ fs. The currents enter the film's interior slightly after the laser's maximum (at $t \approx 4$ fs), as is schematically indicated by the dashed arrows (due to the antisymmetry, the current at the film's center vanishes, giving rise to the white horizontal stripe), and are reflected at the surfaces at $t \approx 12$ fs, leading to a crisscross pattern [see the dashed arrows in Fig. 3(b)]. The spin-resolved currents $j^z_{kl}(t)$ exhibit a pattern (not shown here) reminiscent of that of $j^y_{kl}(t)$ for $p$-polarized light displayed in Fig. 2(e).

The antisymmetry of the observed pattern is apparently related to the symmetry of the sample, in particular to the presence of two identical surfaces. It is understood as a superposition of two patterns with opposite signs, one attributed to the bottom surface and one attributed to the top surface. In experiments, this symmetry is usually broken, for example, by a substrate, thereby leading to disparate surfaces. For this reason, one would observe a superposition of dissimilar patterns or, in the case of thick samples, the pattern attributed to one of the surfaces.

With regard to circularly polarized light, it is sufficient to discuss one helicity (here $\sigma^+$ as defined in Sec. II A) since the $x$ and $z$ components of both spin polarization and spin-resolved currents change sign upon helicity reversal, whereas the $y$ component does not, as confirmed by our simulations.

All components of the site-averaged spin polarization $S^{\mu}(t)$ and the spin-resolved currents $j^{\mu}_{kl}(t)$ are nonzero (Fig. 4, top row). In an admittedly simple picture $S^x(t)$ and $S^z(t)$ may be viewed as being due to the optical orientation in the photoemission [39]. Recall that the laser impinges within the $xz$ plane onto the film; for a single atom optical orientation by circularly polarized light would then cause spin polarization within the $xz$ plane. Likewise, $S^y(t)$ may be attributed to the effect predicted by Tamura *et al.* [4] for SARPES. Of course, this "decomposition of effects" ignores that the superposition of the laser's $s$- and $p$-polarized partial waves is coherent and shifted in phase. Moreover, the electron dynamics mixes the components of the local spin polarization because of spin-orbit coupling; nevertheless, $S^y(t)$ is reminiscent of that for $p$-polarized light [Fig. 2(a)].

As shown in Ref. [40], the spin polarization depends on the angle of incidence and on the photon energy. Moreover, it is strongly energy dependent, with extreme values of up to 0.5 (Fig. 8 in that publication). Averaging over energy in Figs. 8 and 10 in Ref. [40] would yield roughly 0.1, which is larger than but comparable to the maximum values in Fig. 4(a).

### B. fcc Co(100)

For fcc Co(100) we focus on excitation by $p$-polarized light as a representative case (bottom row in Fig. 4; since illumi-

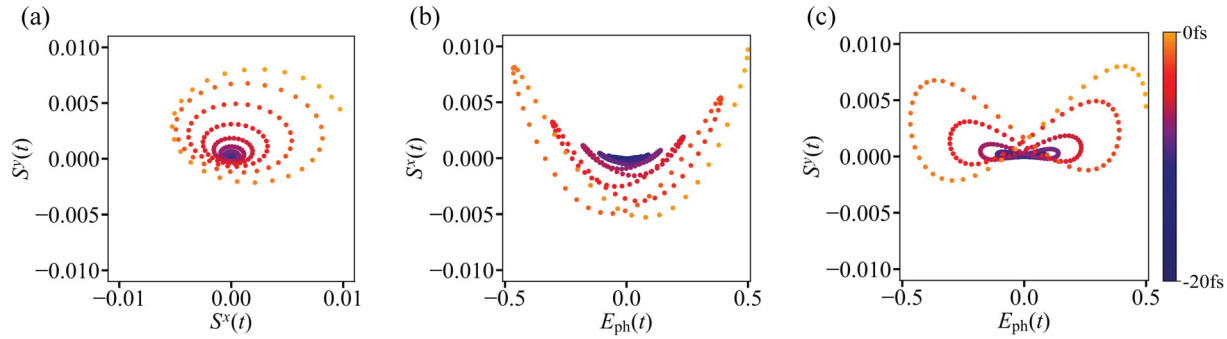


FIG. 5. Laser-driven precession of the spin polarization in Co(100) excited by *p*-polarized light. The color scale visualizes the time evolution from $t = -20$ fs (dark blue) to $t = 0$ fs (orange). (a) Correlation of $S^y(t)$ and $S^x(t)$ using data presented in Fig. 4(e). (b) and (c) show $S^x(t)$ and $S^y(t)$ versus the electric field $E_{\rm ph}(t)$ of the laser pulse, respectively.

nation by circularly polarized light produced similar results, we refrain from discussing those results). As expected and often found in both experiment and theory, the site-averaged spin-polarization component $S^z(t)$ associated with magnetism is reduced by the laser pulse; that is, the sample becomes demagnetized (see Refs. [19,20] and references therein). This demagnetization is site dependent (not shown), similar to the induced spin polarization in Cu(100) discussed before.

In contrast to nonmagnetic Cu(100), the magnetization of Co(100) breaks the mirror symmetry at the $xz$ plane and allows for nonzero $S^x(t)$ and $S^y(t)$ (see Table II). Both components are modulated with the doubled laser frequency but shifted in phase [Fig. 4(e)]. Their magnitudes are roughly 10 % of the $S^y$ component in Cu(100) [Fig. 2(a)]. Moreover, both $S^x(t)$ and $S^y(t)$ of Co(100) exhibit a beating pattern (with maxima at about $t \approx 0$, 10, and 20 fs), while $S^y(t)$ of Cu(100) displays a clear sinusoidal shape.

The spin-polarization components $S^x(t)$ and $S^y(t)$ exhibit a regular pattern before the maximum of the laser pulse [Fig. 4(e)], which hints at laser-driven precession of the spin polarization $\boldsymbol{S}(t)$. Indeed, $S^x(t)$ and $S^y(t)$ display a left-handed helix, starting at the origin, with increasing amplitude [Fig. 5(a)]. Moreover, the noticeable shift of the spiral center to positive values is explained by spin-orbit coupling: a minimal tight-binding model for the motion of $\boldsymbol{S}(t)$, including spin-orbit coupling, yields two features, a deformation of the precession cone and a shift of the cone axis off the magnetization direction ($z$ axis). Without spin-orbit coupling, one finds the usual circular cone with its axis along the magnetization direction.

The time sequences of $S^x(t)$ and $S^y(t)$ versus the laser amplitude $E_{\rm ph}(t)$ prove that the precession is driven by the laser [Figs. 5(b) and 5(c)]. The variations in the patterns are attributed to the phase shift between $S^x(t)$ and $S^y(t)$.

The striking differences in the spin polarization of Cu and Co could be due to the occupation of the electronic states, to spin-orbit coupling, or to exchange splitting. In order to shed light upon the origin we performed simulations for Cu and Co in which the number of initially occupied states, the strength of the spin-orbit coupling, and the exchange splitting were varied (not shown here). While the former two have a minute effect on the spin polarization in both Cu and Co, reducing the exchange splitting removes the rapid oscillations and preserves the long-period oscillations that are observed in Co(100) [Fig. 4(e)]. These findings prompt exchange splitting as the main origin.

As for the spin polarization, all three components of the spin-resolved currents are nonzero [Figs. 4(f)–4(h)], with the $z$-component $j^z_{kl}(t)$ being the largest, as exhibited by darker colors in Fig. 4(h). All components oscillate in unison before the laser pulse maximum; complicated current patterns arise after the pulse.

Summarizing briefly for Cu and Co, we find that the simulations confirm the symmetry considerations. General trends are unison oscillations before the laser maximum and complicated patterns thereafter; the optically induced spin-polarization components are smaller in a magnetic sample but exhibit precession before the laser pulse maximum.

### C. Co/Cu heterostructure

We now address a Co/Cu(100) heterostructure illuminated by *p*-polarized light. Decomposing $S^x(t)$ and $S^y(t)$ of the entire sample [black lines in Figs. 6(a) and 6(b)] into the respective parts in the Co (cyan) and Cu (magenta) regions indicates that $S^x(t)$ [Fig. 6(a)] is first induced by the laser pulse in the Co region and subsequently enters the Cu region [recall that $S^x(t)$ is symmetry forbidden in Cu(100); see Sec. III A]. This finding underlines the importance of an interface for ultrafast spin dynamics.

In contrast, $S^y(t)$ is by far the largest in the nonmagnetic Cu region [Fig. 6(b)], whereas it is strongly reduced in the Co region. This finding corroborates the above argument that magnetism may reduce photoinduced spin-polarization components. Both the magnitude and frequency of the site-averaged components in the two regions are reminiscent of those in the respective homogeneous samples.

The currents $j_{kl}(t)$ exhibit an oscillating collective motion across the sample before the pulse, similar to Cu(100) [Fig. 2(c)]. However, beginning slightly before the pulse maximum at $t = 0$ fs, the spatial homogeneity is lost; instead there are sizable currents initiated at the interface (visualized by the horizontal dashed line at site 19) and propagating toward the Co region [dark blue features in Fig. 6(c)]. This finding corroborates that the interface acts as a "source" of ultrafast spin currents. At the magnetic/nonmagnetic interface, the imbalance of occupation facilitates the production of currents. Moreover, since the imbalance is spin dependent,

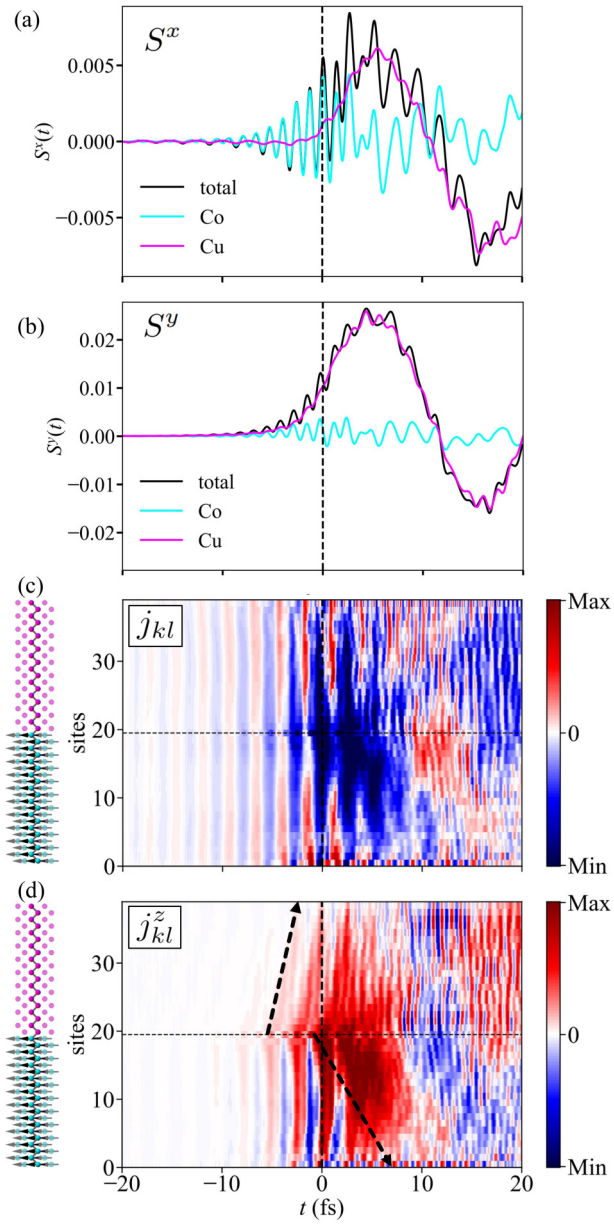


FIG. 6. Photoinduced spin polarization and currents of a Co/Cu(100) heterostructure excited by $p$-polarized light. (a) Component $S^x(t)$ of the site-averaged spin polarization (black) decomposed into that in the Co region (cyan) and that in the Cu region (magenta). The latter are normalized with respect to $N_{\text{site}}$ [see Eq. (7)]. The maximum of the laser pulse at $t = 0$ fs is marked by the vertical dashed line. (b) The same as (a), but for $S^y(t)$. (c) Currents $j_{kl}(t)$ depicted as a color scale (red is positive; blue is negative). The Co/Cu interface is identified by the horizontal dashed line. (d) The same as (c), but for spin-resolved currents $j^z_{kl}(t)$. Arrows serve as a guide to the eye.

the spin-resolved currents $j^z_{kl}(t)$, that is, those with spin along the magnetization direction, should also be triggered at the interface. This is, indeed, verified by $j^z_{kl}(t)$ [Fig. 6(d)]. More precisely, these currents are homogeneous in the Co region before the pulse; they become enhanced at the interface at about $t = -5$ fs (dark red patches; also illustrated by the black arrows). The $x$- and $y$-spin-resolved currents (not shown here) are not affected as much by the interface as the $z$ component, which suggests that the imbalance of magnetization (spin-dependent occupation) at the interface is the most relevant origin.

The above argument concerning the importance of interfaces is further supported by the varying velocities of $j^z_{kl}(t)$ in the Cu and Co regions (approximately 2.8 nm/fs in Cu and 0.9 nm/fs in Co [see the inclinations of the arrows in Fig. 6(d)]; these velocities compare well with those computed for other materials, e.g., in Refs. [17,41]). In the latter, we find the homogeneous oscillating current pattern before the pulse maximum. In the Cu region, which is nonmagnetic, the same pattern appears oblique, as indicated by the black dashed arrows in Fig. 6(d). This means that these currents spill out from the Co region into the Cu region and propagate toward the Cu surface (site 39).

## IV. CONCLUSION AND OUTLOOK

Our theoretical findings suggest that femtosecond laser pulses impinging on thin films may be used to generate ultrafast oscillating spin-polarized currents. Moreover, interfaces amplify the production of these currents, as is evidenced in our study. And the spin polarization can be tuned by details of the laser's electric field, in particular by the polarization of the radiation.

Inhomogeneities in the sample (surfaces, interfaces) yield intrinsic imbalances of occupation which facilitate the production of spin-polarized currents. This finding supports reasoning given in Ref. [42], in which it was argued that a spin-dependent imbalance of occupation, termed spin voltage in that paper, results in both demagnetization and spin currents.

Spin pumping is the transfer of spin from a ferromagnet into an attached normal metal due to precession of the local magnetic moments in the ferromagnet. Extending this picture, fluctuations of local magnetic moments may also cause the effect [43,44]. Assuming a fixed collinear magnetic structure, based on electron dynamics rather than on magnetization dynamics, the transfer of spin found in the presented simulations does not fall into this category of spin pumping but, nevertheless, may be termed "spin pumping" in a general sense. Hence, our study gives further details on the mechanisms for the transfer of spin polarization across a magnetic/normal metal interface generated by laser excitation, as reported, for example, in Refs. [14,17,45,46].

As shown in this paper, already the combination of 3$d$ materials (here Co and Cu) produces sizable spin-polarization effects. The latter could be enhanced further by increasing the imbalance of spin-dependent occupation at interfaces. Material combinations worth investigating could comprise heavier elements with larger spin-orbit coupling (e.g., Pt [40]) and heavy magnetic materials (e.g., Gd).

A direct observation of the photoinduced spin polarization and the spin-polarized currents studied in this paper challenges experiments because of their as yet limited temporal resolution. However, it is conceivable to probe the currents via their emitted electromagnetic radiation (see, for example, Ref. [47]).

We conclude by discussing the advantages and disadvantages of the EVOLVE framework. The real-space approach gives access to spatiotemporal distributions of observables with atomic and femtosecond resolution. Being an effective one-electron approach, large samples and long time spans can be simulated; in contrast, *ab initio* approaches are limited in sample size and time interval but are more accurate (e.g., Ref. [48]). Moreover, EVOLVE is flexible: interactions (e.g., spin-orbit coupling and exchange splitting) can be varied deliberately, one can choose closed or open boundary conditions along individual directions, and samples may contain inhomogeneities (e.g., defects or interfaces, noncollinear magnetic textures). For thermalization (i.e., relaxation from an excited state toward the thermal ground state) that occurs on a timescale of a few hundred femtoseconds, coupling to a bosonic heat bath can be turned on [19,20].

Electron-electron scattering is currently not explicitly included in the simulations but may be added in the Hartree-Fock approximation. The validity of the presented results is therefore somewhat limited, even when focusing on the period of a laser excitation. Since the electron-electron interaction is reflected partially in the tight-binding parameters (for the ground state), only deviations from the ground state's occupation profile need to be considered. We expect attraction and repulsion within the dynamic spatial charge distribution that is generated by the laser pulse. For example, the electron-electron interaction could reduce the propagation length of currents (attractive interaction) or spread regions with increased or decreased occupation (repulsive interaction), both of which could diminish the coherence in occupation and current profiles.

## ACKNOWLEDGMENT

This work is funded by the Deutsche Forschungsgemeinschaft (DFG, German Research Foundation), Project ID No. 328545488–TRR 227, project B04.

[1] S. Hüfner, *Photoelectron Spectroscopy: Principles and Applications*, 2nd ed. (Springer, Berlin, 1996).
[2] *Solid-State Photoemission and Related Methods*, edited by W. Schattke and M. A. Van Hove (Wiley-VCH, Weinheim, 2003).
[3] J. Henk, K. Miyamoto, and M. Donath, Phys. Rev. B **98**, 045124 (2018).
[4] E. Tamura, W. Piepke, and R. Feder, Phys. Rev. Lett. **59**, 934 (1987).
[5] E. Tamura and R. Feder, Solid State Commun. **79**, 989 (1991).
[6] E. Tamura and R. Feder, Europhys. Lett. **16**, 695 (1991).
[7] J. Henk and R. Feder, Europhys. Lett. **28**, 609 (1994).
[8] J. Henk, T. Scheunemann, S. V. Halilov, and R. Feder, J. Phys.: Condens. Matter **8**, 47 (1996).
[9] K. Starke, *Magnetic Dichroism in Core-Level Photoemission* (Springer, Berlin, 2007).
[10] E. Beaurepaire, J.-C. Merle, A. Daunois, and J.-Y. Bigot, Phys. Rev. Lett. **76**, 4250 (1996).
[11] G. P. Zhang and W. Hübner, Phys. Rev. Lett. **85**, 3025 (2000).
[12] G. Zhang, W. Hübner, E. Beaurepaire, and J.-Y. Bigot, in *Spin Dynamics in Confined Magnetic Structures I*, edited by B. Hillebrands and K. Ounadjela (Springer, Berlin, 2003), p. 245.
[13] J. Hermanson, Solid State Commun. **22**, 9 (1977).
[14] M. Battiato, K. Carva, and P. M. Oppeneer, Phys. Rev. Lett. **105**, 027203 (2010).
[15] M. Battiato, K. Carva, and P. M. Oppeneer, Phys. Rev. B **86**, 024404 (2012).
[16] M. Battiato, P. Maldonado, and P. M. Oppeneer, J. Appl. Phys. **115**, 172611 (2014).
[17] D. M. Nenno, B. Rethfeld, and H. C. Schneider, Phys. Rev. B **98**, 224416 (2018).
[18] S. Kaltenborn, Y.-H. Zhu, and H. C. Schneider, Phys. Rev. B **85**, 235101 (2012).
[19] F. Töpler, J. Henk, and I. Mertig, New J. Phys. **23**, 033042 (2021).
[20] F. Ziolkowski, O. Busch, I. Mertig, and J. Henk, J. Phys.: Condens. Matter **35**, 125501 (2023).
[21] B. Heinrich, Z. Celinski, K. Myrtle, J. F. Cochran, M. Kowalewski, A. S. Arrott, and J. Kirschner, J. Appl. Phys. **69**, 5217 (1991).
[22] M. J. Mehl and D. A. Papaconstantopoulos, Phys. Rev. B **54**, 4519 (1996).
[23] C.-S. Yoo, P. Söderlind, and H. Cynn, J. Phys.: Condens. Matter **10**, L311 (1998).
[24] J. C. Slater and G. F. Koster, Phys. Rev. **94**, 1498 (1954).
[25] D. A. Papaconstantopoulos, *Handbook of the Band Structure of Elemental Solids* (Springer, Berlin, 2015).
[26] S. Konschuh, M. Gmitra, and J. Fabian, Phys. Rev. B **82**, 245412 (2010).
[27] A. V. Kimel, A. Kirilyuk, P. A. Usachev, R. V. Pisarev, A. M. Balbashov, and T. Rasing, Nature (London) **435**, 655 (2005).
[28] R. Hertel, J. Magn. Magn. Mater. **303**, L1 (2006).
[29] S. B. Mishra and S. Coh, Phys. Rev. B **107**, 214432 (2023).
[30] S. Savasta and R. Girlanda, Solid State Commun. **96**, 517 (1995).
[31] G. D. Mahan, *Many-Particle Physics*, 3rd ed. (Springer, New York, 2000).
[32] B. K. Nikolić, L. P. Zârbo, and S. Souma, Phys. Rev. B **73**, 075303 (2006).
[33] M. D. Petrović, B. S. Popescu, U. Bajpai, P. Plecháč, and B. K. Nikolić, Phys. Rev. Appl. **10**, 054038 (2018).
[34] *Spin–Orbit-Influenced Spectroscopies of Magnetic Solids*, edited by H. Ebert and G. Schütz (Springer, Berlin, 1996).
[35] See Supplemental Material at http://link.aps.org/supplemental/10.1103/PhysRevB.108.184401 for animations of the spin dynamics.
[36] In the spirit of a two-current model one may write $j_x = j_x^{\uparrow_y} + j_x^{\downarrow_y}$ and $j_x^y = j_x^{\uparrow_y} - j_x^{\downarrow_y}$ for the spin-integrated current $j_x$ and the $y$-spin-polarized current $j_x^y$, respectively. Denoting the spin orientation $\uparrow_y$ ($\downarrow_y$) as the majority (minority) orientation with respect to the $y$ direction, the finding is attributed to a flow of minority-spin electrons.
[37] R. Feder, *Polarized Electrons in Surface Physics* (World Scientific, Singapore, 1986).

[38] J. Kirschner, *Polarized Electrons at Surfaces* (Springer, Berlin, 1985).
[39] J. Kessler, *Polarized Electrons*, 2nd ed. (Springer, Berlin, 1985).
[40] C. M. Schneider and J. Kirschner, Crit. Rev. Solid State Mater. Sci. **20**, 179 (1995).
[41] V. P. Zhukov, E. V. Chulkov, and P. M. Echenique, Phys. Rev. B **73**, 125105 (2006).
[42] R. Rouzegar, L. Brandt, L. Nádvorník, D. A. Reiss, A. L. Chekhov, O. Gueckstock, C. In, M. Wolf, T. S. Seifert, P. W. Brouwer, G. Woltersdorf, and T. Kampfrath, Phys. Rev. B **106**, 144427 (2022).
[43] Y. Tserkovnyak, A. Brataas, and G. E. W. Bauer, Phys. Rev. Lett. **88**, 117601 (2002).
[44] Y. Tserkovnyak, A. Brataas, and G. E. W. Bauer, Phys. Rev. B **66**, 224403 (2002).
[45] M. Battiato, Ph.D. thesis, Uppsala Universitet, 2013.
[46] A. Alekhin, I. Razdolski, N. Ilin, J. P. Meyburg, D. Diesing, V. Roddatis, I. Rungger, M. Stamenova, S. Sanvito, U. Bovensiepen, and A. Melnikov, Phys. Rev. Lett. **119**, 017202 (2017).
[47] T. Kampfrath, M. Battiato, P. Maldonado, P. G. Eilers, J. Nötzold, S. Mährlein, V. Zbarsky, F. Freimuth, Y. Mokrousov, S. Blügel, M. Wolf, I. Radu, P. M. Oppeneer, and M. Münzenberg, Nat. Nanotechnol. **8**, 256 (2013).
[48] J. K. Dewhurst, P. Elliott, S. Shallcross, E. K. U. Gross, and S. Sharma, Nano Lett. **18**, 1842 (2018).